PAPER • OPEN ACCESS

False signatures of non-ergodic behavior in disordered quantum many-body systems

IOP Publishing New J. Phys. 27 (2025) 125001 https://doi.org/10.1088/1367-2630/ae20b3

New Journal of Physics
The open access journal at the forefront of physics

Deutsche Physikalische Gesellschaft DPG
IOP Institute of Physics

Published in partnership with: Deutsche Physikalische Gesellschaft and the Institute of Physics

PAPER

False signatures of non-ergodic behavior in disordered quantum many-body systems

Adith Sai Aramthottil[1,2], **Ali Emami Kopaei**[1,2], **Piotr Sierant**[3], **Lev Vidmar**[4,5] and **Jakub Zakrzewski**[2,6,*]

[1] Szkoła Doktorska Nauk Ścisłych i Przyrodniczych, Uniwersytet Jagielloński, Łojasiewicza 11, PL-30-348 Kraków, Poland
[2] Instytut Fizyki Teoretycznej, Wydział Fizyki, Astronomii i Informatyki Stosowanej, Uniwersytet Jagielloński, Łojasiewicza 11, PL-30-348 Kraków, Poland
[3] Barcelona Supercomputing Center, Barcelona 08034, Spain
[4] Department of Theoretical Physics, J. Stefan Institute, SI-1000 Ljubljana, Slovenia
[5] Department of Physics, Faculty of Mathematics and Physics, University of Ljubljana, SI-1000 Ljubljana, Slovenia
[6] Mark Kac Complex Systems Research Center, Uniwersytet Jagielloński, Kraków, Poland
[*] Author to whom any correspondence should be addressed.

E-mail: jakub.zakrzewski@uj.edu.pl

Keywords: ergodicity, chaos, localization, disorder

OPEN ACCESS

RECEIVED
30 July 2025

REVISED
16 November 2025

ACCEPTED FOR PUBLICATION
18 November 2025

PUBLISHED
1 December 2025

Abstract

Ergodic isolated quantum many-body systems satisfy the eigenstate thermalization hypothesis (ETH), i.e. the expectation values of local observables in the system's eigenstates approach the predictions of the microcanonical ensemble. However, the ETH does not specify what happens to expectation values of local observables within an energy window when the average over disorder realizations is taken. As a result, the expectation values of local observables can be distributed over a relatively wide interval and may exhibit nontrivial structure, as shown in Aramthottil *et al* (2021 *Phys. Rev. B* **104** 214201) for a quasiperiodic disordered system for site-resolved magnetization. We argue that the non-Gaussian form of this distribution may *falsely* suggest non-ergodicity and a breakdown of ETH. By considering various types of disorder, we find that the functional forms of the distributions of matrix elements of the site-resolved magnetization operator mirror the distribution of the onsite disorder. We argue that this distribution is a direct consequence of the local observable having a finite overlap with moments of the Hamiltonian. We then demonstrate how to adjust the energy window when analyzing expectation values of local observables in disordered quantum many-body systems to correctly assess the system's adherence to ETH, and provide a link between the distribution of expectation values in eigenstates and the outcomes of quench experiments.

1. Introduction

The fundamental postulates of thermodynamics for closed systems are a consequence of ergodicity, wherein a system explores all accessible microstates within its phase space over long times, allowing physical observables to be determined as ensemble averages with respect to appropriate statistical ensembles [1, 2]. While the attempts to define ergodicity of quantum systems date back to the early days of quantum mechanics and von Neumann's ergodic theorem [3], the definition of ergodicity of quantum many-body systems, in the form of the eigenstate thermalization hypothesis (ETH), was developed only several decades later [4]. Initially, the progress was restricted to semi-classical systems exhibiting classical chaos. In such systems, the eigenvalue statistics were argued to follow the predictions of random matrix theory [5–7], in contrast to the Poissonian statistics observed in classically integrable systems.

A leap in our understanding of quantum ergodicity for closed systems was made in [8], where considering a simple Hamiltonian with many disconnected sectors perturbed by a random matrix coupling led to mixing of a large number of states within a small energy range. This resulted in ergodic eigenstates that have expectations similar to those of the microcanonical ensemble. The questions of quantum

ergodicity were also considered by [9–12], which led to the introduction [13–15] of the ETH ansatz

$$\langle n|\hat{\mathcal{O}}|m\rangle = \mathcal{O}\left(\bar{E}\right)\delta_{mn} + \mathrm{e}^{-S\left(\bar{E}\right)/2} f\left(\bar{E},\omega\right) R_{mn}, \tag{1}$$

where $|m\rangle, |n\rangle$ are the eigenstates of the given Hamiltonian and E_n and E_m are the corresponding eigenvalues, $\bar{E} = (E_m + E_n)/2, \omega = E_m - E_n$. Here, $\mathcal{O}(\bar{E})$ is the expectation value of the microcanonical ensemble, while $f(\bar{E},\omega)$ controls the functional form of thermalization; smooth functions approximate both. For time-reversal symmetry, R_{mn} is a random real variable with zero mean and unit variance $\overline{R_{mn}^2} = 1$, while $S(\bar{E})$ is the thermodynamic entropy at energy $\bar{E}$, i.e. the logarithm of the density of states (DoS) [16]. Numerical investigations have extensively verified the ETH, ranging from the smoothness of the expectation value of the operator to the exponential decay in off-diagonal elements of the operator with system size, across a diverse range of nonintegrable quantum many-body systems [15, 17–36]. Recently, the notions of quantum ergodicity and ETH were connected [37–40] with the ideas of unitary designs [41] and the theory of free probability [42]. The most important object for our work here is the smooth function $\mathcal{O}(\bar{E})$ (we set $\bar{E} \to E$ further on), which was argued in [43] to encode the overlap of the Hamiltonian with conserved quantities, including the higher moments of the Hamiltonian.

In this work, we focus on the ETH in disordered many-body systems and pose the question of how to perform the disorder average of the equation (1) to extract meaningful information about the quantum ergodicity of the system. We first demonstrate that disorder can lead to anomalous distributions of matrix elements for certain observables, which may be misinterpreted as evidence for the breakdown of the ETH. We then argue that this problem is intimately connected to the way the energy window of the microcanonical ensemble is adjusted to each disorder realization. We analyze the implications of the different choices of the position of the energy window for the resulting distribution of expectation values of local observables, and we show how properties consistent with the ergodic character of the system are restored.

The paper is organized as follows. In section 2, we briefly describe the peculiar properties of the probability distribution of the site-resolved magnetization for the Heisenberg spin$-1/2$ chain in the presence of the quasiperiodic disorder as encountered in [44]. The site resolved magnetization is defined as $\langle n|\hat{s}_l^z|n\rangle \equiv s_l^z$, where $\hat{s}_l^z$ is z-projection of spin 1/2 operator at site l; with l sampled over site indices and aggregated over sites when considering distributions. We proceed to explore the distribution of s_l^z for the Heisenberg spin $-1/2$ chain with different types of onsite disorders. This leads us to a conjecture about the relationship between the distribution of the onsite disorder and the properties of the s_l^z distribution. We show the validity of this conjecture by finding the leading-order approximation for the microcanonical expectation of the site-resolved magnetization in section 3, and conclude that the particular structure of the s_l^z distribution is an artifact of the choice of the energy window, section 4. Finally, in section 5, we show that these specific structures have direct consequences for experiments and can be detected in the time dynamics of the s_l^z expectation values.

2. Unusual distribution for the site-resolved magnetization

We begin with a brief description of the distribution of site-resolved magnetization in a Heisenberg spin-1/2 chain (HSC) with quasiperiodic disorder [44]. The HSC is a paradigmatic model extensively employed to study ergodicity breaking and the interplay between disorder and quantum many-body dynamics [45]. The HSC Hamiltonian with open boundary conditions in the presence of an onsite potential reads

$$\hat{H}_{\mathrm{HSC}} = \sum_{l=1}^{L-1}\left(\hat{s}_l^x\hat{s}_{l+1}^x + \hat{s}_l^y\hat{s}_{l+1}^y + \hat{s}_l^z\hat{s}_{l+1}^z\right) + \sum_{l=1}^{L} h_l\hat{s}_l^z, \tag{2}$$

where $\hat{s}_l^\alpha$ are spin-1/2 operators acting on site l, with $\alpha \in x,y,z$ and L is the system size. Disorder in the model arises from the onsite potential term; initially, we shall consider an example of disorder arising from a quasiperiodic potential (**QP**) [46]. The model has a $U(1)$ symmetry leading to magnetization, $M \equiv \sum_{l=1}^{L}\hat{s}_l^z$, being conserved. We will restrict ourselves to the magnetization-zero sector in this work. The QP introduces a deterministic, incommensurate modulation in the onsite potential, given by:

$$h_l = W\cos\left(2\pi\beta l + \phi\right), \tag{3}$$

where β is an irrational number, frequently chosen as the inverse golden ratio, $\beta = (\sqrt{5}-1)/2$, ensuring the potential lacks periodicity for typical finite L. The phase ϕ is drawn randomly from a uniform distribution, $\phi \in [0, 2\pi)$, with each value of ϕ corresponding to a distinct disorder

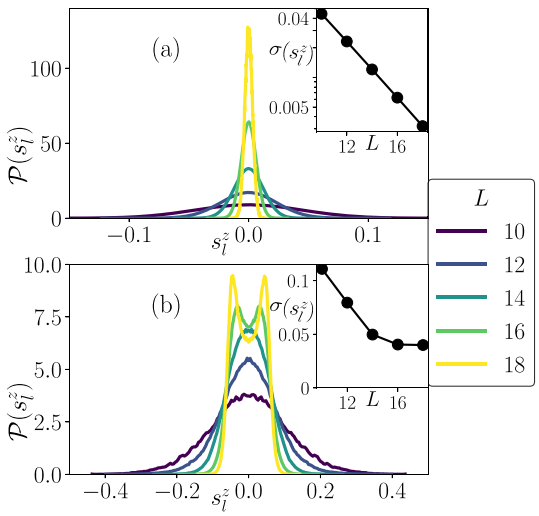

Figure 1. The probability distribution of site-resolved magnetization, s_l^z, for disorder-averaged GOE matrices (a) and the HSC-QP Hamiltonian at $W = 0.5$ (b) at different system sizes, L. For both (a) and (b) panels, 100 eigenstates are considered at the rescaled energy $\epsilon = 0.5$. The number of disorder realizations is varied, being at least 7500 for $L \leqslant 16$ and 60 for $L = 18$ for panel (a), while for HSC-QP case (b) it is 10^4 disorder realizations for $L \leqslant 16$ and 2500 for $L = 18$. The insets show the standard deviations of respective distributions, decreasing exponentially with L for GOE (a) and saturating for HSC-QP model.

realization. At a strong onsite potential, the system is in the non-ergodic, many-body localized (MBL), regime [45, 47–49] which, at system sizes and timescales relevant to experimental and numerical considerations, arises for $W_c \geqslant 2$ [44, 50]. Interestingly, such a QP disorder appears often in experimental implementations of the disorder [51–55]. In the remainder of this work, however, we focus on the regime of weak disorder, $W \ll W_c$, in which the system is ergodic and possesses level statistics characteristic of the Gaussian orthogonal ensemble (GOE) of random matrices [56, 57].

Analysis of the properties of matrix elements $\langle n|\hat{\mathcal{O}}|n\rangle$ of the observable $\hat{\mathcal{O}}$ requires fixing an energy window to which the eigenvalues E_n belong. This energy window is commonly rescaled with the system size, L, to facilitate comparisons across different system sizes and scales, as detailed in prior works such as [58]. In a more rigorous framework, particularly in the context of studies exploring the MBL phenomenon, a definition of rescaled energy values was proposed in [59, 60]. This approach provides a way of comparing properties of the system at different energies by defining the rescaled energy ϵ as:

$$\epsilon = \frac{E - E_{\text{min}}}{E_{\text{max}} - E_{\text{min}}}, \tag{4}$$

where E represents the energy of the state under consideration, while E_{min} and E_{max} denote the minimum and maximum eigenvalues in the spectrum, respectively. This definition ensures that ϵ is normalized to the range $[0, 1]$.

The observable of interest in this work is the site-resolved magnetization, $\hat{\mathcal{O}} \equiv \hat{s}_l^z$. In analogy with a random matrix, one could expect the observable to be Gaussian distributed around its mean value and with a standard deviation that is exponentially decreasing with system size. We confirm this expectation numerically by taking the Hamiltonian $\hat{H}$ as a matrix from the GOE [56]. The dimension of H is the same as the Hilbert space dimension of HSC; the diagonal matrix elements of H are taken from the Gaussian distribution $\mathcal{N}(0, 1)$ with zero mean and unity variance, while the off-diagonal elements of H are taken from $\mathcal{N}(0, 1/2)$. In figure 1(a), we show the probability distribution of site-resolved magnetization considering the expectation values $s_l^z = \langle n|\hat{s}_l^z|n\rangle$ in eigenstates $|n\rangle$ around the rescaled energy $\epsilon = 0.5$. We observe a clear single peak structure with the standard deviation decreasing exponentially with system size.

A different result is obtained for the HSC Hamiltonian with QP disorder for eigenstates around $\epsilon = 0.5$, that is, eigenstates in the middle of the spectrum. In this case, the distributions were found [44] to have a peculiar double-peak structure in the ergodic regime. With increasing system size, the double peak structure was found to be more prominent, as shown in figure 1(b). This result raises the question: Is it a signature of the ETH breakdown, or is it a peculiar property of the disorder distribution?

We note that a similar behavior was found for the difference in the site-resolved magnetization of adjacent sites $\delta s_l^z \equiv s_{l+1}^z - s_l^z$. [44] hinted at characteristic relationship of the distribution of s_l^z with that of adjacent onsite potential difference, $\delta h_l \equiv h_{l+1} - h_l$, which for QP takes the probability distribution

form $\mathcal{P}(\delta h_l) = (2W\pi \sin(\pi\beta))^{-1}(1-(\delta h_l/(2W\sin(\pi\beta)))^2)^{-1/2}$ with $\delta h_l \in [-2W\sin(\pi\beta), 2W\sin(\pi\beta)]$ having peaks at $\delta h_l = \pm 2W\sin\pi\beta$. We point out here that the onsite fields h_l also have a probability distribution $\mathcal{P}(h_l) = (W\pi)^{-1}(1-(h_l/W)^2)^{-1/2}$ with peaks at $\pm W$.

Motivated by the intuitions from [44] that the distributions of s_l^z or δs_l^z have similar characteristics to those of h_l or δh_l, we here explore the probability distribution of site-resolved magnetization and its differences. In particular, we examine various kinds of disorder and contrast it with the distribution of the onsite disorder and its differences for the following potentials:

1. Random disorder (RD): in this case, the onsite potentials h_l are sampled independently from a uniform box distribution:

$$h_l \in [-W, W], \tag{5}$$

   where W denotes the disorder strength. The RD introduces spatially uncorrelated variations in the potential landscape. This model, at considered system sizes, is in the MBL regime at a sufficiently strong disorder. In figures 2(a), (f) and 3(a), (f), we see that the distribution of s_l^z also has a regime where it is flat, resembling the distribution of h_l, while the distribution of δs_l^z shares features with the triangle distribution of δh_l.
2. Cosine disorder: it arises via randomizing the QP in equation (3) by choosing the phase $\phi_l \in [0, 2\pi)$ independently at each lattice site l, [61], resulting in

$$h_l = W\cos(2\pi\beta l + \phi_l). \tag{6}$$

   The HSC with this disorder type is in the MBL regime for $W \geqslant 2.5$ [61]. The cosine disorder as shown in figures 2(b), (g) and 3(b), (g) has similar structure of disorder to quasiperiodic one with singular values at the end for $\mathcal{P}(h_l)$. In the ergodic regime of HSC this leads to double peaks appearing in the site-resolved spin expectation values s_l^z. At the same time, the distribution of the difference of the on-site potential $\mathcal{P}(\delta h_l)$ differs and shows just a single peak centered around zero. Correspondingly, the distribution of the difference of site-resolved spin expectation values (δs_l^z) shows a single peak.
3. Binary disorder: we consider here a distribution with equal probability $h_l = -W$ and $h_l = W$. The model is in the MBL regime for disorder strength $W_c \geqslant 1.25$ [62]. We show in figures 2(c), (h) and 3(c), (h) that the distributions of s_l^z in the ergodic regime of this model are characterized by strong double peaks resembling the binary distribution of h_l. Analogous behavior occurs for δs_l^z, which has a distribution similar to the distribution of δh_l, with three peaks, with one in the middle with a prominent amplitude.
4. Tertiary disorder: we consider a distribution of disorder with h_l selected randomly, with equal probability, to be $h_l \in \{-W, 0, W\}$. This model is in the MBL regime for $W_c \geqslant 1.25\sqrt{\frac{3}{2}}$ [62]. In figures 2(d), (i) and 3(d), (i), we show the presence of triple peaks in the s_l^z distribution, associated with the tertiary distribution of h_l, while δh_l has a quinary distribution and correspondingly δs_l^z has 5 peaks with amplitudes decreasing with the distance from $|\delta s_l^z| = 0$.
5. Triangle-wave quasiperiodic disorder: we consider here a spatially correlated disorder of the form

$$h_l = W\left[2\left|2\left(\frac{(2\pi\beta l+\phi)}{2\pi} - \left\lfloor\frac{(2\pi\beta l+\phi)}{2\pi} + \frac{1}{2}\right\rfloor\right)\right| - 1\right], \tag{7}$$

   where β is the inverse golden ratio. As shown in figures 2(e), (j) and 3(e), (j), this disorder has the peculiar property of h_l being distributed uniformly, resulting in s_l^z admitting a flat-top distribution form similar to RD, while the distribution of δh_l has singularities at the edges of the distribution corresponding to double peaks for δs_z^l.

The numerical analyses from figures 2 and 3 confirm the inference of [44]: for each type of disorder, the site-resolved magnetization (or its difference between neighboring sites) has a distribution that closely resembles the features of the distribution of on-site disorder (or its differences between neighboring sites). These features are inconsistent with the distribution of expectation values of local observables in highly excited eigenstates based on random matrix theory, see figure 1(a), and hence may be interpreted as inconsistent with the ergodicity of the system. The remainder of this manuscript is devoted to understanding the origin and the implications of these *false* signatures of non-ergodicity in the ergodic regime of disordered many-body systems.

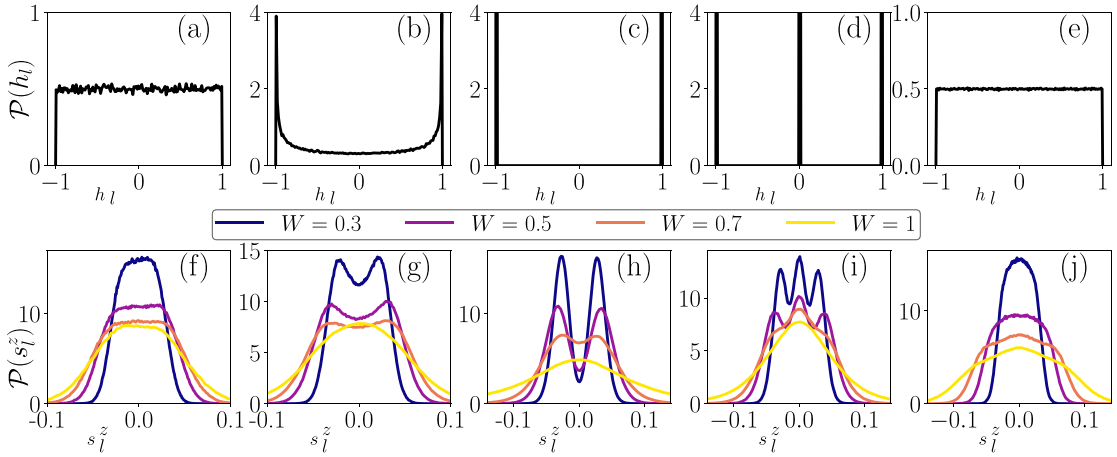

Figure 2. The distribution of onsite disorder is depicted for various types of disorders, including random (a), cosine (b), binary (c), tertiary (d), and triangle-wave (e). Additionally, the corresponding distributions of site-resolved magnetization are shown in (f)–(j), considering 100 states near $\epsilon = 0.5$ averaged over at least 200 disorder realizations for a system of size $L = 18$.

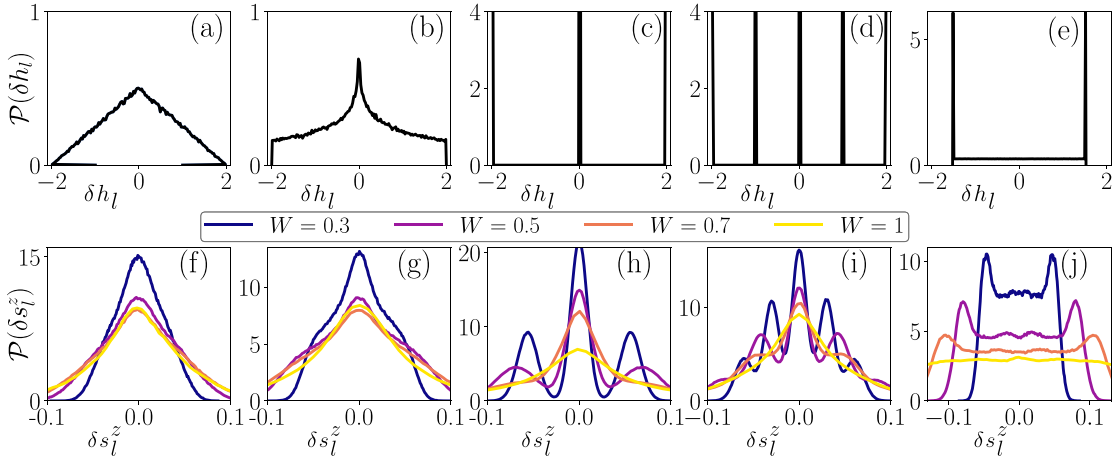

Figure 3. The distribution of the difference of adjacent onsite disorder, δh_l, is depicted for various types of disorders, including random (a), cosine (b), binary (c), tertiary (d), and triangle-wave (e). Additionally, the corresponding distributions of differences of adjacent site-resolved magnetization, δs_l^z, (f)–(j), considering 100 states near $\epsilon = 0.5$, averaged over at least 200 disorder realizations for a system of size $L = 18$.

3. Microcanonical expectation for site-resolved magnetization

In this section, we argue that the apparent signatures of non-ergodicity in the disorder-averaged distributions of matrix elements of local observables—shown in the bottom rows of figures 2 and 3—originate from the interplay between the energy dependence of $\mathcal{O}(E)$ in the ETH ansatz (1) and the choice of energy window ($\epsilon = 0.5$) used in the analysis.

To proceed more formally, following [43] we define the Hilbert–Schmidt product in operator space as $\langle \hat{A}, \hat{B} \rangle \equiv \frac{1}{D}\mathrm{Tr}[\hat{A}^\dagger \hat{B}]$, where D is the Hilbert space dimension, and the norm as $||\hat{A}|| = \sqrt{\langle \hat{A}, \hat{A} \rangle}$. The Hamiltonian of an ergodic many-body system is denoted by $\hat{H}$, and $\hat{\mathcal{O}}$ represents an arbitrary few-body observable. The operator space can be decomposed into two orthogonal subspaces: one spanned by the powers of the Hamiltonian, $\hat{H}^k$ (with $k \geqslant 0$), and an orthogonal complement. Hence, the observable $\hat{\mathcal{O}}$ can be decomposed as

$$\hat{\mathcal{O}} = \hat{\mathcal{O}}_{\parallel} + \hat{\mathcal{O}}_{\perp}, \tag{8}$$

where $\hat{\mathcal{O}}_{\parallel}$ belongs to the subspace spanned by the moments of the Hamiltonian $\hat{H}^k$, while $\hat{\mathcal{O}}_{\perp}$ lies in the orthogonal complement of this subspace. Assuming that ℓ is the smallest positive integer such that $\hat{H}^{\ell+1}$ is linearly dependent on $\hat{H}^0, \hat{H}, \hat{H}^2, \ldots, \hat{H}^\ell$, the parallel component of the observable of interest can be

uniquely expressed as

$$\hat{\mathcal{O}}_{\parallel} = \sum_{k=0}^{\ell} \gamma_k \hat{H}^k. \tag{9}$$

Substituting equation (9) into equation (8) and evaluating the expectation value in the eigenstate $|n\rangle$ of the Hamiltonian $\hat{H}$, we obtain

$$\langle n|\hat{\mathcal{O}}|n\rangle = \sum_{k=0}^{\ell} \gamma_k E_n^k + \langle n|\hat{\mathcal{O}}_{\perp}|n\rangle. \tag{10}$$

To establish a connection between the diagonal matrix element $\langle n|\hat{\mathcal{O}}|n\rangle$ and the smooth function $\mathcal{O}(E)$ in the ETH ansatz (1), it is necessary to understand the behavior of $\langle n|\hat{\mathcal{O}}_{\perp}|n\rangle$.

By definition, since $\hat{\mathcal{O}}_{\parallel}$ is a linear combination of the powers of the Hamiltonian $\hat{H}$, we have $[\hat{H}, \hat{\mathcal{O}}_{\parallel}] = 0$. Therefore, the operator $\hat{\mathcal{O}}_{\perp}$ encodes the components of the observable $\hat{\mathcal{O}}$ that do not commute with the Hamiltonian. In particular, when $||[\hat{H}, \hat{\mathcal{O}}]|| = O(1)$, the norm of $\hat{\mathcal{O}}_{\perp}$ is also of order unity, $||\hat{\mathcal{O}}_{\perp}|| = O(1)$. To bound $\langle n|\hat{\mathcal{O}}_{\perp}|n\rangle$ in equation (10), we invoke properties of ergodic systems. While $\hat{\mathcal{O}}_{\perp}$ is a nontrivial operator, it bears no special relationship to the eigenvectors $|n\rangle$ of the Hamiltonian. If the system is ergodic, $\langle n|\hat{\mathcal{O}}_{\perp}|n\rangle$ can be modeled as a diagonal element of a random matrix scaling as $\langle n|\hat{\mathcal{O}}_{\perp}|n\rangle = O(1/\sqrt{D})$ and, therefore, exponentially with the system size, L. In this case, equation (10) implies that $\langle n|\hat{\mathcal{O}}|n\rangle$ becomes, up to $O(e^{-L})$ corrections, a smooth function of energy, leading to

$$\mathcal{O}(E) = \sum_{k=0}^{\ell} \gamma_k E^k. \tag{11}$$

In passing, we note that the influence of integrals of motion beyond the moments of the Hamiltonian, $\hat{H}^k$, can be systematically taken into account, as shown in [43].

Let us now specialize to the observable of interest, i.e. the site-resolved magnetization, $\hat{s}_l^z$, and as the Hamiltonian consider $\hat{H}_{\mathrm{HSC}}$. From equation (11), we observe that understanding of the microcanonical expectation value $s_l^z(E)$ requires evaluation of the coefficients γ_k. Moreover, for a system with near-Gaussian DoS with a variance proportional to the system size (see appendix B) and an operator with norm independent of the system size, it was observed [43] that taking only the first p terms in the expansion (9), incurs an error decreasing with system size L as $O(1/L^{p-1})$. For this reason, we consider only the first two terms in the expansion $\hat{s}_{l,\parallel}^z = \gamma_0 \hat{H}_{\mathrm{HSC}}^0 + \gamma_1 \hat{H}_{\mathrm{HSC}}^1$, resulting in

$$\hat{s}_l^z = \gamma_0 \mathbb{I} + \gamma_1 \hat{H}_{\mathrm{HSC}} + \hat{s}_{l,\perp}^z. \tag{12}$$

Calculating the Hilbert–Schmidt product $\langle \mathbb{I}, \hat{s}_l^z \rangle$ in (12), we find that

$$\frac{1}{D}\mathrm{Tr}\left(\hat{s}_l^z\right) = \gamma_0 + \gamma_1 \frac{1}{D}\mathrm{Tr}\left(\hat{H}_{\mathrm{HSC}}\right), \tag{13}$$

while, by computing $\langle H_{\mathrm{HSC}}, \hat{s}_l^z \rangle$ in (12), we obtain that

$$\frac{1}{D}\mathrm{Tr}\left(\hat{H}_{\mathrm{HSC}}\hat{s}_l^z\right) = \gamma_0 \frac{1}{D}\mathrm{Tr}\left(\hat{H}_{\mathrm{HSC}}\right) + \gamma_1 \frac{1}{D}\mathrm{Tr}\left(\hat{H}_{\mathrm{HSC}}^2\right). \tag{14}$$

In both steps, we used the fact that $\hat{s}_{l,\perp}^z$ is orthogonal to $\hat{H}_{\mathrm{HSC}}^k$ for any integer $k \geqslant 0$. Directly computing $\mathrm{Tr}(s_l^z) = 0$, $\mathrm{Tr}(\hat{H}_{\mathrm{HSC}})/D = -1/4$, $\mathrm{Tr}(\hat{H}_{\mathrm{HSC}}\hat{s}_l^z)/D = 1/4h_l - 1/(4(L-1))\sum_{l\neq i} h_i$ and $\mathrm{Tr}(\hat{H}_{\mathrm{HSC}}^2)/D = (3L^2 - 3L - 1)/(16(L-1)) + 1/4\sum_{i=1}^{L} h_i^2 - 1/(4(L-1))\sum_{l\neq j} h_l h_j$, we use equations (13) and (14) to determine the values of γ_0 and γ_1, which, through (11), imply that

$$s_j^z(E) \propto \frac{E + 1/4}{3L/4 + \sum_i h_i^2} h_j = \frac{E - \langle E \rangle}{3L/4 + \sum_i h_i^2} h_j\,, \tag{15}$$

up to $O(1/L)$ corrections. Above, $\langle E \rangle = \frac{1}{D}\mathrm{Tr}(\hat{H}_{\mathrm{HSC}}) = -\frac{1}{4}$. Further details of the derivations may be found in appendix A while the near-Gaussian assumption on the DoS is justified in appendix B.

The derived linear relationship between the site-resolved magnetization, $s_j^z(E)$, and the energy accurately reproduces the behavior of the diagonal matrix element $\langle n|\hat{s}_l^z|n\rangle$ in the Hamiltonian's eigenstates.

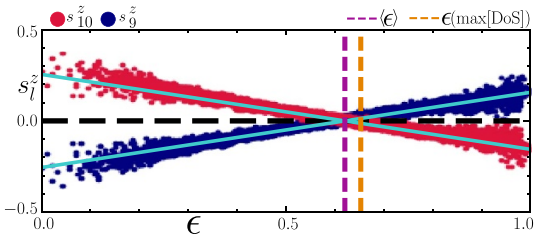

Figure 4. The site-resolved magnetization, s^z_l, for a single disorder realization of the HSC QP model at different rescaled energies ϵ for $L = 18$ and $W = 0.5$. The dark blue and red scatter plots correspond to sites $l = 9$ and $l = 10$. The dashed, vertical lines indicate the rescaled energy values that give the maximum value of DoS and the average rescaled energy $\langle\epsilon\rangle$. The bold blue lines illustrate the analytical curves obtained by expanding the microcanonical expectation value, $\mathcal{O}(\epsilon)$, to the first order in the Hamiltonian's moment.

This is illustrated in figure 4 which shows that $\langle n|\hat{s}^z_l|n\rangle$ concentrate, up to fluctuations suppressed exponentially with system size L, around the curves $s^z_j(E)$ at all values of the rescaled energy ϵ as ascertained in figure 6. Fitting $\langle n|\hat{s}^z_l|n\rangle$ as a function of energy, we confirm that the resulting linear fit reproduces the parameters of (15) down to machine precision. In particular, we observe that the zero of $s^z_l(E)$ occurs at the rescaled energy $\langle\epsilon\rangle$ corresponding to $\langle E\rangle$.

4. Artifacts in disorder averaged observables

The simple approximation for the microcanonical expectation of site-resolved magnetization, (15), establishes a framework to capture the anomalous probability distribution of s^l_z when disorder-averaged properties of the system are considered.

The approximation implies that for a given disorder strength, s^z_l is proportional to the local disorder field h_l and linearly varies with the energy from the point $E = \langle E\rangle$. Consequently, if one considers the eigenstates around an energy significantly distant from $\langle E\rangle$ for different disorder realizations, the s^z_l values will be confined within a width restricted by the energy distance from $\langle E\rangle$, and they will take linearly dependent values proportional to h_l within this width. This scenario is illustrated in figure 5 where we compare the distributions of s^z_l obtained for different energy intervals, one of them being centered at $\langle\epsilon\rangle \approx 0.62$ and two other at $\langle\epsilon\rangle \pm \varepsilon$ with $\varepsilon \approx 0.076$. Already for random uniform disorder, the obtained distributions significantly differ, compare figure 5(a). For QP disorder, the difference is more spectacular, and a double peak structure appears.

Consider now 'corrected' observables $\tilde{s}^z_l = s^z_l - s^z_l(E)$, where $s^z_l(E)$ is the approximation for the microcanonical expectation found by explicitly solving for the first two coefficients in (11). Such a compensation results in a single peak, Gaussian-like distributions for both random uniform and QP disorders, as illustrated in figures 5(c) and (d). We have verified that the residual differences (absent, by the way, in the QP case) can be attributed to finite-size (by a comparison with lower system size results) and low-order truncation effects.

Let us concentrate on eigenstates around $\langle\epsilon\rangle$ where no energy correction to magnetization is necessary and analyze the influence of the system size on the probability distributions for both s^z_l and δs^z_l. Both distributions significantly narrow with the system size, with the associated standard deviation decreasing exponentially with increasing L, as shown in insets in figure 6. The distributions are, to a good approximation, Gaussians for sufficiently large L as apparent from the lower panels plotted in the logarithmic vertical scale. This indicates that the corrections to s^z_l coming from the energy dependence are exponentially decreasing with L, consistently with the expectations based on the random matrix theory, recall figure 1(a).

Within this framework, one can explain the anomalous behavior in figure 1(b), as well as similar observations in [63–65]. The rescaled energy considered in that work, fixed as $\epsilon = 0.5$, significantly deviates from the value of the rescaled energy $\langle\epsilon\rangle \approx 0.62$ corresponding to $\langle E\rangle = -1/4$. Note also that $\langle\epsilon\rangle$ fluctuates between disorder realizations. In effect, one observes non-trivial distributions of the on-site magnetization as in figure 2, where the eigenstates belong to the energy window determined by $\epsilon = 0.5$ sufficiently far from $\langle\epsilon\rangle$ and also fluctuate from one disorder realization to another. The same mechanism can also be extended to linear combinations of site-resolved magnetizations, explaining the characteristics of differences in site-resolved magnetization shown in figure 3.

The interested reader may be puzzled by the dependence of the observed anomalies on disorder amplitude W. Firstly, let us stress that such a behavior may be considered as anomalous when observed

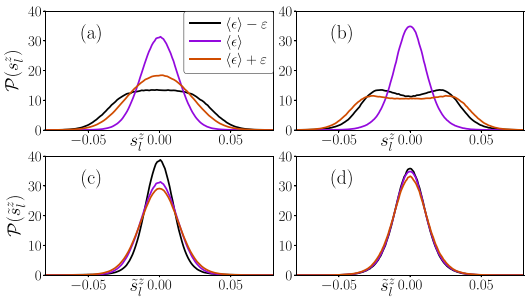

Figure 5. (a), (b) The probability distribution for the site-resolved magnetization, s_l^z, and (c), (d) the site-resolved magnetization after removing the approximate microcanonical expectation, $\tilde{s}_l^z$. Results are shown, respectively, for the HSC model with Random (a), (c) and QP (b), (d) disorder. For all panels $L = 18$, $W = 0.5$, with 100 eigenstates in intervals around $\langle\epsilon\rangle$ and $\langle\epsilon\rangle \pm \varepsilon$ for at least 1300 disorder realizations.

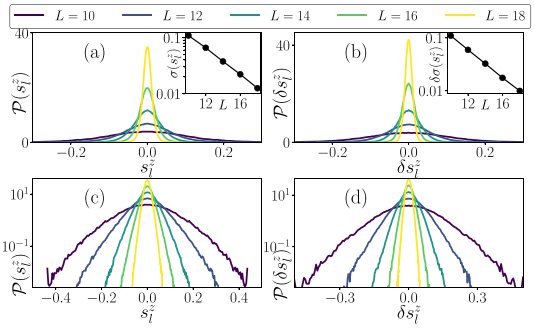

Figure 6. The probability distribution of site-resolved magnetization, s_l^z, (a) and the difference of site-resolved magnetization, δs_l^z, (b) for disorder-averaged HSC-QP Hamiltonian. The insets for (a) and (b) show the standard deviation with system sizes for s_l^z and δs_l^z, respectively. Panels (c) and (d) show the same curves as in (a) and (b) but in a logarithmic vertical scale. The distributions are for $W = 0.5$ considering 100 eigenstates at the average energy $\langle\epsilon\rangle$ with at least 4500 disorder realizations for different system sizes, L.

in the otherwise ergodic regime. For large disorder, close to the crossover to many-body localization, the nonergodic behavior is expected. The small disorder details are discussed in appendix D.

5. Effects on time-dynamics

In this section, we examine the experimental consequences of the anomalous distributions of s_l^z in eigenstates. We consider a system with Hamiltonian $\hat{H}$, initialized in state $|\phi\rangle$ and denote the time-evolved state by $|\phi(t)\rangle = e^{-i\hat{H}t}|\phi\rangle$. The long-time average $\mathcal{O}$ of the expectation value of an observable $\hat{O}$ is given as

$$\begin{aligned}\mathcal{O} &\equiv \lim_{T\to\infty} \frac{1}{T}\int_0^T dt \langle\phi(t)|\hat{\mathcal{O}}|\phi(t)\rangle \\ &= \lim_{T\to\infty} \frac{1}{T}\int_0^T dt\, e^{i(E_m - E_n)t} \sum_{m,n} \langle m|\hat{\mathcal{O}}|n\rangle c_m^* c_n, \end{aligned} \tag{16}$$

where $c_n = \langle n|\phi\rangle$. Performing the time integral, we note that only the diagonal terms, $m = n$, yield a non-vanishing contribution, showing that $\mathcal{O}$ is given by the expectation value in the *diagonal ensemble,*

$$\mathcal{O} = \sum_n \langle n|\hat{\mathcal{O}}|n\rangle |c_n|^2, \tag{17}$$

defined by the initial state $|\phi\rangle$. When the $\hat{H}$ is ergodic and local, and the initial state is a product state, the energy fluctuations are subextensive [4], $\delta E_\phi / E_\phi \sim 1/\sqrt{L}$, where $E_\phi = \langle\phi|\hat{H}|\phi\rangle$ and $\delta E_\phi = \sqrt{\langle\phi|\hat{H}^2|\phi\rangle - E_\phi^2}$. In that case, the diagonal ensemble expectation value, (17), may be close to the microcanonical average $\mathcal{O}(E_\phi)$, (1), at energy E_ϕ. In an ergodic disordered system, the mechanism leading to the *false* signatures of non-ergodicity in the distributions of expectation values of local

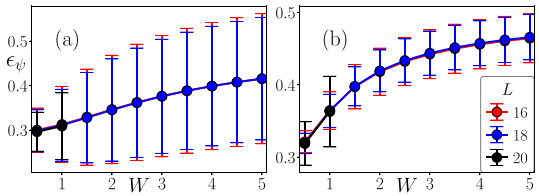

Figure 7. The disorder averaged rescaled energy expectation value for the Néel state, ϵ_ψ, and the associated standard deviation with disorder realization (shown here by the error bars) varying with disorder strength for different system sizes. For the HSC Hamiltonian with RD (a) and QP disorder (b). Both (a) and (b) consider 2500 disorder realizations.

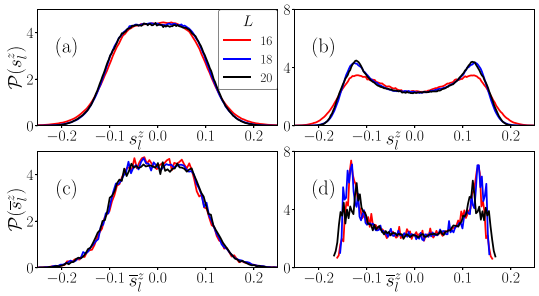

Figure 8. The probability distribution of site-resolved magnetization of eigenstates, $\mathcal{P}(s_l^z)$, for different system sizes around energies $\langle\psi|\hat{H}|\psi\rangle$, the expectation energy of the Néel state for both the RD (a) and QP (b) case. Both (a) and (b) consider 100 eigenstates for at least 1000 disorder realizations with $W = 0.5$. The bottom row provides a comparison with the distributions for site-resolved magnetization at long times obtained from dynamics of the initial Néel state, $\mathcal{P}(\bar{s}_l^z)$ again for both RD (c) and QP (d) disorder cases. Both (c) and (d) consider 2500 disorder realizations.

observables in eigenstates may lead to a non-trivial spread of the long-time averages, equation (16), of the local observables. In the following, we analyze this effect on the example of disordered HSC, showing how to assess the ergodicity of the system correctly.

We fix the initial quench state as the Néel state $|\psi\rangle \equiv |\uparrow\downarrow\cdots\uparrow\downarrow\rangle$ and follow the time evolution for individual disorder realizations using Chebyshev propagation scheme [66]—see appendix C. For disorder strength $W = 0.5$, the average rescaled energy of $|\psi\rangle$ in the HSC model with both the RD and QP disorder is $\langle\psi|\hat{H}_{\rm HSC}|\psi\rangle \equiv \epsilon_\psi \approx 0.3$, see Figure 7. The latter value is significantly distant from the rescaled energy $\langle\epsilon\rangle \approx 0.62$ corresponding to $\langle E\rangle = -1/4$. At the considered system size, the expectation value $\hat{s}_l^z$ enters a stationary regime already at time-scales $O(100)$. Hence, as an approximation for the infinite time average in equation (16) for the operator $\hat{s}_l^z = \hat{\mathcal{O}}$, we consider its long time average as

$$\bar{s}_l^z \equiv \frac{1}{t_2 - t_1}\int_{t_1}^{t_2} \langle\psi|\hat{s}_l^z(t)\,|\psi\rangle \mathrm{d}t. \tag{18}$$

where we take $t_1 = 200$ and $t_2 = 2000$. For the considered HSC, and for the operator $\hat{\mathcal{O}} = \hat{s}_l^z$, the long time average approximates accurately (for this choice of t_1, t_2 up to errors of the order $O(10^{-4})$) the diagonal ensemble expectation value given by (17). Hence, in the following, we are using the diagonal ensemble and the long-time average of the $\hat{s}_l^z$ operator interchangeably. We show in figure 8 that the probability distribution obtained from the long-time average of $\bar{s}_l^z$ over disorder realizations has similar characteristics to that found from eigenstates at energies corresponding to the initial energy of the Néel state for each disorder realization. In particular, for the HSC-QP model, $\mathcal{P}(\bar{s}_l^z)$ reveals a double peak structure, with similar widths of the side peaks for $L = 16, 18$ while being broader for $L = 20$, which reflects the standard deviations in ϵ_ψ (see figure 7). With increasing system size the orthogonal fluctuation to the microcanonical expectation, $\langle n|\hat{O}_\perp|n\rangle$, exponentially decreases, leading to better approximations of the peaks in $\mathcal{P}(\bar{s}_l^z)$ by the distribution $\mathcal{P}(s_l^z)$.

The distributions of $\bar{s}_l^z$, obtained from the simulated time dynamics for different sites l and disorder realizations, do not follow a naive expectation of their narrow concentration around the mean value equal to zero for disordered ergodic systems. As shown in figure 9, these distributions are centered around the microcanonical ensemble expectation value, $s_l^z(E_\psi)$ calculated at the energy E_ψ of the initial Néel state, up to corrections decreasing with system size L. This microcanonical ensemble expectation value is estimated as an average of s_l^z over N eigenstates with eigenenergies close to a desired energy $s_l^z(E) = 1/N\sum_n \langle n|\hat{s}_l^z|n\rangle$.

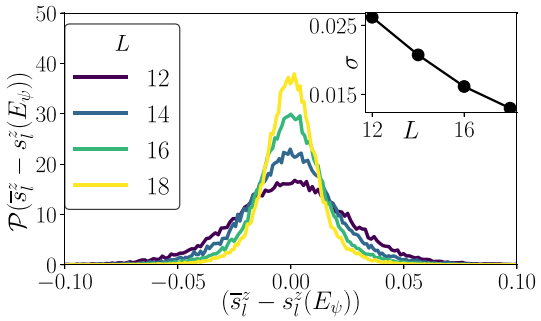

Figure 9. The probability distribution of long time average of the site-resolved magnetization, $\overline{s}_l^z$, (18), corrected by the microcanonical expectation value, $s_l^z(E_\psi)$, in the Néel state, $\mathcal{P}(\overline{s}_l^z - s_l^z(E_\psi))$, for the HSC Hamiltonian with RD for different system sizes. The microcanonical expectation is calculated as an average over 10 eigenstates, and the probability distributions are found by considering 2500 disorder realizations.

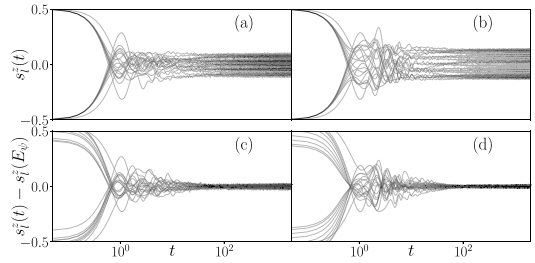

Figure 10. The time dynamics of the site-resolved magnetizations, $s_l^z(t) = \langle\psi|\hat{s}_l^z(t)|\psi\rangle$, for the Néel initial evolved state with the HSC Hamiltonian and RD, (a) or QP (b) disorders for a single disorder realization with $W = 0.5$ and the system size $L = 20$. Each black curve represents a different site magnetization $s_l^z(t)$. The bottom row shows the same dynamics when the microcanonical expectation for each spin, $s_l^z(E_\psi)$ (obtained using 100 eigenstates) is subtracted, $\tilde{s}_l^z \equiv s_l^z(t) - s_l^z(E_\psi)$.

Similarly to the case of eigenstates considered earlier, the significant spread of the long-time averages, $\overline{s}_l^z$, may lead to *false* conclusions about the breakdown of ergodicity. A remedy for this artifact may be, however, readily constructed, even at the single disorder realization level. Instead of analyzing the long-time dynamics for individual spin, $s_l^z(t) = \langle\psi|\hat{s}_l^z(t)|\psi\rangle$, one may subtract from it the microcanonical expectation. The result of such a procedure can be seen in figure 10. The top row presents different $s_l^z(t)$ for a single disorder realization, showing the residual spread of the saturation values, $\overline{s}_l^z$, present even at long times. When $\tilde{s}_l^z(t) = s_l^z(t) - s_l^z(E_\psi)$ are plotted, the spread dramatically narrows down, and $\tilde{s}_l^z(t)$ fluctuates, at long times, around zero mean, as one could expect for the ergodic dynamics.

6. Conclusion

In this study, we have highlighted the subtle issues related to self-averaging in disorder-averaged observables, focusing on the experimentally relevant probe of site-resolved magnetization in spin-1/2 chains. Taking as an example the paradigmatic HSC, we systematically investigated various types of onsite disorder in the ergodic regime. Our results show that the nontrivial structures observed in the probability distributions of matrix elements of local observables arise as a direct consequence of the energy dependence of the microcanonical expectation value, which varies for each specific disorder realization. Importantly, we demonstrated that the expected Gaussian behavior predicted by random matrix theory can be recovered either by selecting eigenstates near the infinite-temperature energy window or by explicitly removing the mean microcanonical contribution. This work clarifies how misleading signatures of non-ergodic behavior can emerge and provides practical guidance for correctly interpreting numerical and experimental results in disordered quantum systems.

Furthermore, we have shown that these microcanonical artifacts persist in experimentally relevant long-time dynamics and can lead to false signatures of non-self-averaging behavior if not properly accounted for. Our results highlight the necessity of carefully distinguishing true ergodicity-breaking effects from energy-window artifacts when interpreting both numerical and experimental observations.

Data availability statement

All data that support the findings of this study are available at RODBUK UJ repository and available at https://doi.org/10.57903/UJ/BCYX1B.

Acknowledgments

A S A, P S, and J Z would like to acknowledge insightful discussions with Titas Chanda in the initial stages of this work. We also thank Konrad Pawlik for a careful reading of the manuscript. The work of A S A and J Z was partially funded by the National Science Centre, Poland, project 2021/03/Y/ST2/00186 within the QuantERA II Programme (DYNAMITE) that has received funding from the European Union Horizon 2020 research and innovation programme under Grant Agreement No 101017733 and by the National Science Centre, Poland, project 2021/43/I/ST3/01142 – OPUS call within the WEAVE programme. A E K acknowledges the support of the National Science Centre, Poland, via Project No. 2021/42/A/ST2/00017. P S acknowledges fellowship within the 'Generación D' initiative, Red.es, Ministerio para la Transformación Digital y de la Función Pública, for talent attraction (C005/24-ED CV1), funded by the European Union NextGenerationEU funds, through PRTR. L V acknowledges support from the Slovenian Research and Innovation Agency (ARIS), Research core funding Grants No. P1-0044, No. N1-0273, and No. J1-50005. We gratefully acknowledge the Polish high-performance computing infrastructure PLGrid (HPC Centers: ACK Cyfronet AGH) for providing computer facilities and support within the computational Grant No. PLG/2025/018400.

Appendix A. Traces for γ_0 and γ_1

Let us start by decomposing the Heisenberg spin-1/2 chain (HSC) Hamiltonian with onsite fields as a sum of 2−site and 1−site local operators. Leading to the expression for the Hamiltonian as $\hat{H}_{\rm HSC} \equiv \sum_{i=1}^{L-1}[\hat{J}_{i,i+1} + \hat{V}_{i,i+1}] + \sum_{i=1}^{L}\hat{h}_i$, where $\hat{J}_{i,i+1} \equiv \frac{1}{2}(\hat{s}_i^+\hat{s}_{i+1}^- + \hat{s}_i^-\hat{s}_{i+1}^+)$, $\hat{V}_{i,i+1} = \hat{s}_i^z\hat{s}_{i+1}^z$ and $\hat{h}_i \equiv h_i\hat{s}_i^z$. Considering the zero magnetization sector in the $Z-$basis, which has a dimension $D = L!/((L/2)!(L/2)!)$, we will estimate the various traces of interest associated with the derivations of γ_0 and γ_1. That is, $\mathrm{Tr}[\hat{s}_l^z]$, $\mathrm{Tr}[\hat{H}_{\rm HSC}]$, $\mathrm{Tr}[\hat{H}_{\rm HSC}^2]$ and $\mathrm{Tr}[\hat{s}_l^z\hat{H}_{\rm HSC}]$.

It is immediately apparent that $\mathrm{Tr}[\hat{s}_l^z]$ is simply zero, so we start by calculating the trace of the Hamiltonian, $\mathrm{Tr}[\hat{H}_{\rm HSC}]$. The tunneling terms, $\hat{J}_{i,i+1}$, here will only have off-diagonal elements and thus do not contribute to the Hamiltonian trace. From $\mathrm{Tr}[\hat{s}_l^z] = 0$ it is evident that the contributions from the onsite fields $\hat{h}_i$ are also zero. And the only terms that contribute are the interaction terms $\hat{V}_{i,i+1}$ which from the combinatorial restrictions associated with choosing two spins oriented in up/down directions within this magnetization restricted basis make a contribution $\mathrm{Tr}[\hat{J}_{i,i+1}] = -D/(4(L-1))$. Thus, considering all terms for the HSC Hamiltonian with open boundary conditions, one gets: $\mathrm{Tr}[\hat{H}_{\rm HSC}] = -D/4$.

Next, considering the higher moment of the Hamiltonian, $\mathrm{Tr}[\hat{H}_{\rm HSC}^2]$, one needs to take into account pure squares of the local operators of the Hamiltonian and products of different local operators. The terms of the tunneling part that lead to products with other local operators are once again purely off-diagonal and do not contribute, so one is left with terms of the form $\hat{J}_{i,i+1}^2$ or $\hat{J}_{i,i+1}\hat{J}_{j,j+1}$ (with $i \neq j$) , here again all terms of the second form will only have off-diagonal elements and will have zero contribution. On expanding the trace associated with $\hat{J}_{i,i+1}^2$ one finds $\hat{J}_{i,i+1}^2 = \mathrm{Tr}[(\hat{s}_i^x)^2(\hat{s}_{i+1}^x)^2 + (\hat{s}_i^y)^2(\hat{s}_{i+1}^y)^2 + (\hat{s}_i^x)(\hat{s}_{i+1}^x)(\hat{s}_i^y)(\hat{s}_{i+1}^y) + (\hat{s}_i^y)(\hat{s}_{i+1}^y)(\hat{s}_i^x)(\hat{s}_{i+1}^x)]$. The first two terms here are scalars and will just have the contribution $\mathrm{Tr}[(\hat{s}_i^x)^2(\hat{s}_{i+1}^x)^2 + (\hat{s}_i^y)^2(\hat{s}_{i+1}^y)^2] = D/8$, while for the second term with the Pauli commutation relations one can recover a local operator of the form $\hat{V}_{i,i+1}$; then making use of the combinatorial restrictions one finds $\mathrm{Tr}[(\hat{s}_i^y)(\hat{s}_{i+1}^y)(\hat{s}_i^x)(\hat{s}_{i+1}^x)] = D/(8(L-1))$. On summing over all terms one finds the contribution from the tunneling part as $\mathrm{Tr}[\sum_{i,j}\hat{J}_{i,i+1}\hat{J}_{j,j+1}] = DL/8$. Considering, in turn, the interaction part of the cross-term product with the onsite field operators will have no contribution as it will just produce 3−site or 1−site $\hat{s}_l^z$ operators, both of which have vanishing trace. Now, considering the pure products of the interaction part, one has terms of the form $\mathrm{Tr}[\hat{V}_{i,i+1}\hat{V}_{j,j+1}]$. For $i = j$ the trace will give the scalar contribution $D/16$. While, for $|i-j| = 1$ the trace will take a form $\frac{1}{4}\mathrm{Tr}[\hat{s}_m^z\hat{s}_n^z]$ that makes a contribution $-D/(16(L-1))$. And for $|i-j| > 1$ one has the full 4−site operator of the form $\mathrm{Tr}[\hat{s}_i^z\hat{s}_{i+1}^z\hat{s}_j^z\hat{s}_{j+1}^z]$ that again, making use of combinatorics associated with evaluating the probability of choosing different choices of spins within this constrained basis, gives $\mathrm{Tr}[\hat{s}_i^z\hat{s}_{i+1}^z\hat{s}_j^z\hat{s}_{j+1}^z] = \frac{3D}{16(L-1)(L-3)}$. Summing over all indices the total contribution arising from the interacting part is

$\mathrm{Tr}[\sum_{i,j}\hat{V}_{i,i+1}\hat{V}_{j,j+1}] = L/8 - \frac{1}{16(L-1)}[2(L-2)] + \frac{3D}{16(L-1)(L-3)}[(L-2)(L-3)]$. And finally considering the field terms we find traces of the form $\mathrm{Tr}[h_i\hat{s}_i^z h_j\hat{s}_j^z]$ which when $i=j$ is a trace over a scalar that gives $Dh_i^2/4$ while for $i\neq j$ gives terms similar to $\hat{V}$ and giving the trace value, $\frac{Dh_ih_j}{4(L-1)}$. On summing over indices, $\mathrm{Tr}[\sum_{i,j}\hat{h}_i\hat{h}_j] = +1/4\sum_{i=1}^{L}h_i^2 - 1/(4(L-1))\sum_{i\neq j}h_ih_j$. Collating all contributions from the three terms of the Hamiltonian one finds: $\mathrm{Tr}[\hat{H}_{\mathrm{HSC}}^2]/D = (3L^2-3L-1)/(16(L-1)) + 1/4\sum_{i=1}^{L}h_i^2 - 1/(4(L-1))\sum_{i\neq j}h_ih_j$.

Finally, we look at $\mathrm{Tr}[\hat{H}\hat{s}_j^z]$. This trace just has a trace over local operators, which is up to a constant already dealt with while evaluating $\mathrm{Tr}[\hat{H}_{\mathrm{HSC}}^2]$. Here, there are no contributions from the tunneling and the interaction part based on insights mentioned above. While from the field operators, one gets a trace over operators of the form $\mathrm{Tr}[h_i\hat{s}_i^z\hat{s}_j^z]$, which have already been evaluated up to a scalar above; one finds in the case $i=j$ a contribution of $Dh_i/4$, while for $i\neq j$ the contribution is $-(Dh_i)/(4(L-1))$. Summing over the indices, we find: $\mathrm{Tr}[\hat{H}_{\mathrm{HSC}}\hat{s}_j^z]/D = 1/4h_j - 1/(4(L-1))\sum_{i\neq j}h_i$.

Replacing these traces in (13) and (14) gives the explicit linear form of $\hat{s}_{l,\|}^z$ as

$$\hat{s}_{l,\|}^z = \frac{\left(\frac{1}{4}h_l - \frac{1}{4(L-1)}\sum_{i\neq l}h_i\right)\left[\hat{H}_{\mathrm{HSC}} + 1/4\right]}{\frac{(3L^2-3L-1)}{(16(L-1))} + \frac{1}{4}\sum_i h_i^2 + \frac{1}{4(L-1)}\sum_{i\neq j}h_ih_j - \left(\frac{1}{4}\right)^2}. \tag{A1}$$

Appendix B. Density of states (DoS)

The assumption often made in the context of eigenstate thermalization hypothesis (see, e.g. [43]) is that the DoS is a near-Gaussian with variance that depends linearly on the system size. The DoS is expected to take the particular form

$$\rho(E) \approx \frac{\exp\left(-\frac{(E-\langle E\rangle)^2)}{2\sigma^2}\right)}{\sqrt{2\pi\,\sigma^2}} \tag{B1}$$

with $\sigma^2 \propto L$.

The DoS for the HSC Hamiltonian with random and quasiperiodic potential disorder at the disorder strength we consider, $W=0.5$, is approximately Gaussian with a slight skewness to low energies as shown in figures 11(a) and (b), where the DoS is calculated based on a stochastic Kernel Polynomial approximation method as in [67–69]. Presuming a variance that linearly depends on the system size and

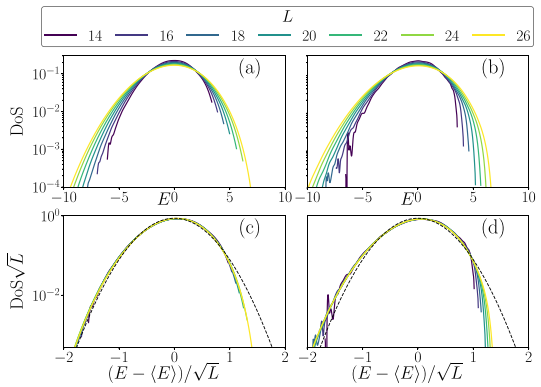

Figure 11. The density of states varying with E for the HSC Hamiltonian with (a) random and (b) quasiperiodic disorder with different system sizes. The panels (c) and (d) correspond to the random and quasiperiodic disorder with the density of states and energies rescaled with a presumed standard deviation $\sqrt{L}$. The dashed line is the expected Gaussian form at very large system sizes as estimated from appendix A. All plots are made for $W=0.5$ considering at least 10 disorder realizations. The DoS are calculated based on a stochastic Kernel Polynomial approximation method using Chebyshev Polynomials as in [67, 68] expanded stochastically to the order of 200 with 200 random vectors.

making appropriate scalings one finds a leading single curve, as shown in figures 11(c) and (d), with additional system size corrections that approaches a Gaussian distribution with increasing system size.

An unskewed Gaussian distribution, as suggested by numericals, is expected for larger system sizes. This is because skeweness, $\gamma = \frac{k_3}{\sigma^3}$, where, k_3 is the third cumulant $k_3 = \langle (H - \langle H \rangle)^3 \rangle$ and expected to grow at maximum as linearly with system size along with variance for a 1 dimensional ergodic Hamiltonian with short range interaction, goes as $\gamma \sim 1/\sqrt{L}$.

Appendix C. Numerical details

The eigenstates and eigenvalues evaluated in the bulk of the spectrum were calculated for system sizes $L \leqslant 18$ either with the standard exact diagonalization (**ED**) method for dense matrices or using the implementation of the shift-invert method in scipy [70]. For $L = 20$ we used the *polynomially filtered exact diagonalization* (**POLFED**) method [69].

The time dynamics considered in figure 8, is obtained using the Chebyshev propagation scheme [66, 71], which approaches the time-evolution operator, $U(\Delta t) = \exp(-iH\Delta t)$, by expansion in terms of the Chebyshev polynomials as

$$U(\Delta t) \approx \left(J_0(a\Delta t) + 2\sum_{k=1}^{N} (-i)^k J_k(a\Delta t)\, T_k(\mathcal{H}) \right) \tag{C1}$$

where, $a = (E_{\max} - E_{\min})/2$, $b = (E_{\max} + E_{\min})/2$ and the Hamiltonian, H, is rescaled as $\mathcal{H} = \frac{1}{a}(H - b)$. Above, $J_k(t)$ is the Bessel function of order k and $T_k(\mathcal{H})$ is the Chebyshev polynomial of order k. The order of expansion N restricts the errors in the time evolution and is determined by a binary search to give values that makes the norm of $U(\Delta t)$ acting on a random normalized state deviating from unity not more than 10^{-13}. For much longer times than we consider in this paper, rigorous numerical comparisons were made with ED for similar systems in [72].

Appendix D. Disorder dependence

There is a simple argument to explain why the resemblance between the magnetization and disorder distributions shown in figures 2 and 3 becomes less and less pronounced as the disorder strength is increased. Consider equation (15), we obtain the approximation

$$s_j^z(E) \propto \frac{E - \langle E \rangle}{3L/4 + \sum_i h_i^2} h_j \approx \frac{E - \langle E \rangle}{L\,(3/4 + W^2\sigma^2)} h_j \tag{D1}$$

where σ^2 is the variance for unit disorder strength, which has a maximum value of $\sigma^2 = 1$ for the binary disorder. Using (D1), one can show that the distribution for $s_j^z(E)$ for a fixed energy and system size gets broader (narrower) if $W < \sqrt{3}/(2\sigma)$ $\left(W > \sqrt{3}/(2\sigma)\right)$. This follows from the fact that taking a typical value of $h_j \approx W\sigma$ we obtain a dispersive curve in (D1)) which reaches extrema at $W = \sqrt{3}/(2\sigma)$. For given values of W in figures 2 and 3, assuming a fixed energy, (D1) one gets broadening distributions.

The eigenstates for figures 2 and 3 were chosen at the rescaled energy $\epsilon = 0.5$, looking at the corresponding energy value E with varying disorder realizations, we find in figure 12 that for random, cosine, binary and tertiary disorders with increasing disorder strength, the energies approach the average energy, $\langle E \rangle = -1/4$, with increasing fluctuations. This leads to the distribution of s_j^z with W becoming progressively smeared from the disorder distribution and eventually losing the peculiar disorder characteristics. For the quasiperiodic triangle wave distribution, there is comparatively less change in energy and fluctuations, leading to a more apparent broadening of the site-resolved magnetization distribution.

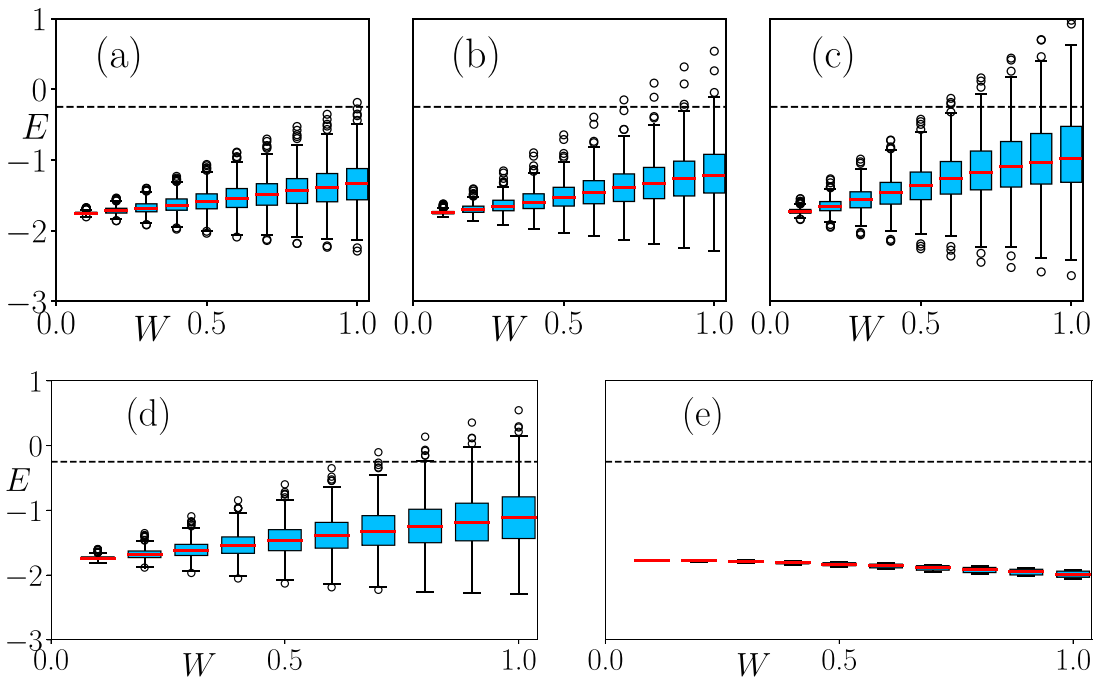

Figure 12. The distribution of energy values corresponding to $\epsilon = 0.5$ over disorder realizations shown with standard box plots for a random (a), cosine (b), binary (c), tertiary (d), and triangle-wave quasiperiodic distribution. The dashed black line corresponds to $\langle E \rangle = -1/4$. All figures consider a system size $L = 18$ with 500 disorder realizations.

ORCID iDs

Lev Vidmar 0000-0002-6641-6653
Jakub Zakrzewski 0000-0003-0998-9460

References

[1] Huang K 2008 *Statistical Mechanics* (Wiley)
[2] Pathria R K 2016 *Statistical Mechanics* (Elsevier)
[3] von Neumann J 2010 *Eur. Phys. J. H* **35** 201
[4] D'Alessio L, Kafri Y, Polkovnikov A and Rigol M 2016 *Adv. Phys.* **65** 239
[5] Berry M V 1977 *J. Phys. A* **10** 2083
[6] Casati G, Valz-Gris F and Guarnieri I 1980 *Lett. Nuovo Cimento (1971-1985)* **28** 279
[7] Bohigas O, Giannoni M J and Schmit C 1984 *Phys. Rev. Lett.* **52** 1
[8] Deutsch J M 1991 *Phys. Rev. A* **43** 2046
[9] Peres A 1984 *Phys. Rev. A* **30** 504
[10] Feingold M, Moiseyev N and Peres A 1984 *Phys. Rev. A* **30** 509
[11] Jensen R V and Shankar R 1985 *Phys. Rev. Lett.* **54** 1879
[12] Feingold M and Peres A 1986 *Phys. Rev. A* **34** 591
[13] Srednicki M 1994 *Phys. Rev. E* **50** 888
[14] Srednicki M 1999 *J. Phys. A: Math. Gen.* **32** 1163
[15] Rigol M, Dunjko V and Olshanii M 2008 *Nature* **452** 854 E
[16] Burke P C and Haque M 2023 *Phys. Rev. E* **107** 034125
[17] Rigol M 2009 *Phys. Rev. Lett.* **103** 100403
[18] Santos L F and Rigol M 2010 *Phys. Rev. E* **81** 036206
[19] Ikeda T N, Watanabe Y and Ueda M 2013 *Phys. Rev. E* **87** 012125
[20] Steinigeweg R, Herbrych J and Prelovšek P 2013 *Phys. Rev. E* **87** 012118
[21] Khatami E, Pupillo G, Srednicki M and Rigol M 2013 *Phys. Rev. Lett.* **111** 050403
[22] Beugeling W, Moessner R and Haque M 2014 *Phys. Rev. E* **89** 042112
[23] Sorg S, Vidmar L, Pollet L and Heidrich-Meisner F 2014 *Phys. Rev. A* **90** 033606
[24] Steinigeweg R, Gemmer J and Brenig W 2015 *Phys. Rev. B* **91** 104404
[25] Mondaini R and Rigol M 2015 *Phys. Rev. A* **92** 041601
[26] Beugeling W, Moessner R and Haque M 2015 *Phys. Rev. E* **91** 012144
[27] Mondaini R, Fratus K R, Srednicki M and Rigol M 2016 *Phys. Rev. E* **93** 032104
[28] Yoshizawa T, Iyoda E and Sagawa T 2018 *Phys. Rev. Lett.* **120** 200604
[29] Jansen D, Stolpp J, Vidmar L and Heidrich-Meisner F 2019 *Phys. Rev. B* **99** 155130
[30] Schönle C, Jansen D, Heidrich-Meisner F and Vidmar L 2021 *Phys. Rev. B* **103** 235137
[31] Noh J D 2023 *Phys. Rev. E* **107** 014130

[32] LeBlond T, Mallayya K, Vidmar L and Rigol M 2019 *Phys. Rev. E* **100** 062134
[33] LeBlond T and Rigol M 2020 *Phys. Rev. E* **102** 062113
[34] Richter J, Dymarsky A, Steinigeweg R and Gemmer J 2020 *Phys. Rev. E* **102** 042127
[35] Brenes M, Goold J and Rigol M 2020 *Phys. Rev. B* **102** 075127
[36] Brenes M, LeBlond T, Goold J and Rigol M 2020 *Phys. Rev. Lett.* **125** 070605
[37] Pappalardi S, Foini L and Kurchan J 2022 *Phys. Rev. Lett.* **129** 170603
[38] Pappalardi S, Fritzsch F and Prosen T 2025 *Phys. Rev. Lett.* **134** 140404
[39] Pappalardi S, Foini L and Kurchan J 2024 *Quantum* **8** 1227
[40] Fava M, Kurchan J and Pappalardi S 2025 *Phys. Rev. X* **15** 011031
[41] Dankert C, Cleve R, Emerson J and Livine E 2009 *Phys. Rev. A* **80** 012304
[42] Voiculescu D 1991 *Invent. math.* **104** 201
[43] Mierzejewski M and Vidmar L 2020 *Phys. Rev. Lett.* **124** 040603
[44] Aramthottil A S, Chanda T, Sierant P and Zakrzewski J 2021 *Phys. Rev. B* **104** 214201
[45] Sierant P, Lewenstein M, Scardicchio A, Vidmar L and Zakrzewski J 2025 *Rep. Prog. Phys.* **88** 026502
[46] Iyer S, Oganesyan V, Refael G and Huse D A 2013 *Phys. Rev. B* **87** 134202
[47] Nandkishore R and Huse D A 2015 *Annu. Rev. Condens. Matter Phys.* **6** 15
[48] Alet F and Laflorencie N 2018 *C. R. Physique* **19** 498
[49] Abanin D A, Altman E, Bloch I and Serbyn M 2019 *Rev. Mod. Phys.* **91** 021001
[50] Falcão P R N, Aramthottil A S, Sierant P and Zakrzewski J 2024 *Phys. Rev. B* **110** 184209
[51] Schreiber M, Hodgman S S, Bordia P, Lüschen H P, Fischer M H, Vosk R, Altman E, Schneider U and Bloch I 2015 *Science* **349** 842
[52] Bordia P, Lüschen H P, Hodgman S S, Schreiber M, Bloch I and Schneider U 2016 *Phys. Rev. Lett.* **116** 140401
[53] Bordia P, Lüschen H, Scherg S, Gopalakrishnan S, Knap M, Schneider U and Bloch I 2017 *Phys. Rev. X* **7** 041047
[54] Lüschen H P, Bordia P, Scherg S, Alet F, Altman E, Schneider U and Bloch I 2017 *Phys. Rev. Lett.* **119** 260401
[55] Lüschen H P, Scherg S, Kohlert T, Schreiber M, Bordia P, Li X, Das Sarma S and Bloch I 2018 *Phys. Rev. Lett.* **120** 160404
[56] Mehta M L 1990 *Random Matrices* (Elsevier)
[57] Haake F 2010 *Quantum Signatures of Chaos* (Springer)
[58] Kim H, Ikeda T N and Huse D A 2014 *Phys. Rev. E* **90** 052105
[59] Luitz D J, Laflorencie N and Alet F 2015 *Phys. Rev. B* **91** 081103
[60] Luitz D J, Laflorencie N and Alet F 2016 *Phys. Rev. B* **93** 060201
[61] Khemani V, Sheng D N and Huse D A 2017 *Phys. Rev. Lett.* **119** 075702
[62] Janarek J, Delande D and Zakrzewski J 2018 *Phys. Rev. B* **97** 155133
[63] Hopjan M and Heidrich-Meisner F 2020 *Phys. Rev. A* **101** 063617
[64] Hopjan M, Orso G and Heidrich-Meisner F 2021 *Phys. Rev. B* **104** 235112
[65] Laflorencie N, Lemarié G and Macé N 2020 *Phys. Rev. Res.* **2** 042033
[66] Fehske H and Schneider R 2008 *Computational Many-Particle Physics* (Springer) (available at: http://dx.doi.org/10.1007/978-3-540-74686-7)
[67] Silver R N and Röder H 1994 *Int. J. Mod. Phys. C* **5** 735
[68] Silver R, Roeder H, Voter A and Kress J 1996 *J. Comput. Phys.* **124** 115
[69] Sierant P, Lewenstein M and Zakrzewski J 2020 *Phys. Rev. Lett.* **125** 156601
[70] Virtanen P *et al* SciPy 1.0 Contributors 2020 *Nat. Methods* **17** 261
[71] Sierant P, Lazo E G, Dalmonte M, Scardicchio A and Zakrzewski J 2021 *Phys. Rev. Lett.* **127** 126603
[72] Sierant P and Zakrzewski J 2022 *Phys. Rev. B* **105** 224203